J Solid State Electrochem (2012) 16:291–295
DOI 10.1007/s10008-011-1333-8

ORIGINAL PAPER

Pb-sandwiched nanoparticles as anode material for lithium-ion batteries

Zhongxue Chen · Yuliang Cao · Jiangfeng Qian · Xinping Ai · Hanxi Yang

Received: 25 December 2010 / Revised: 30 January 2011 / Accepted: 5 February 2011 / Published online: 22 February 2011

Abstract A sandwiched SiC@Pb@C nanocomposite was prepared through a simple ball-milling route and characterized by X-ray diffraction, X-ray photoelectron spectroscopy, scanning electron microscopy, and transmission electron microscopy. The SiC@Pb@C nanocomposite exhibits a much improved reversible capacity and cycling life as compared with a bare Pb anode. A reversible volumetric capacity of >1,586 mAh cm^{-3} (207 mAh g^{-1}) can be maintained after 600 cycles of charge and discharge in the potential interval between 0.005 and 1.0 V, which far exceeds those reported previously in the literature. The enhanced electrochemical performance is ascribed to the sandwiched structure in which nanosized Pb particles were anchored in between the rigid SiC core and the outer carbon shell, mitigating the damage done by the large volume change of the Pb interlayer during the alloying/dealloying process.

Keywords Lithium-ion batteries · Nanocomposite · Ball milling · Anodic materials · Electrochemical performance

Introduction

Lithium-storable metals and alloys, especially those composed of group IVA elements (Si, Ge, Sn, and Pb), have been actively revisited in recent years as alternative anode materials for Li-ion batteries because of their high gravimetric and volumetric capacity compared with graphite [1–3]. In the past few years, much interest has been focused on Li–Si [4–6] and Li–Sn alloys [7–9], and great success has been achieved in upgrading the cycling life of the Sn- and Si-based anodes to hundreds of cycles [6, 8]. Less attention has been devoted to other Li-storable alloys such as Li–Pb, although Pb can also offer high volumetric capacity (6,487 mAh cm^{-3}) eight times that of commercial graphite and a suitable working voltage (0.5–0.7 V) slightly above lithium deposition potential.

A problem common to all group IVA metals when used as lithium alloy anodes is their poor cyclability caused by their large volumetric changes during the alloying/dealloying process [10, 11]. Additionally, the solid electrolyte interface (SEI) film that forms on the surface of Pb-based anodes during the initial cycle is unstable, leading to poorer charge–discharge efficiency at prolonged cycling [12, 13]. Several strategies have been proposed to enhance the capacity retention of Pb anode, including decreasing the particle size [14] and dispersing Pb into an inactive matrix [15, 16]. Liu and Lee [15] reported an amorphous $Pb_3P_2O_8$ anode with consistent cycling performance and demonstrated the feasibility of a lithium phosphate matrix to cushion the volume change during insertion and extraction of lithium. Pan t al. [16] fabricated a core–shell PbO@C that exhibited a reversible capacity of 170 mAh g^{-1} after the 50th cycle.

Recently, we developed a sandwiched nanostructure to obtain highly cycleable Sn and Sb nanocomposites with a rigid SiC nanocore, metal interlayer, and graphite outer layer [17, 18]. The work recounted in this paper was aimed at extending this synthetic strategy to a similar group IVA element, Pb, to develop a cyclable Pb anode material for lithium alloy–dealloy reaction. Here, we report the synthet-

Z. Chen · Y. Cao (✉) · J. Qian · X. Ai · H. Yang (✉)
Hubei Key Laboratory of Electrochemical Power Sources,
Department of Chemistry, Wuhan University,
Wuhan 430072, China
e-mail: ylcao@whu.edu.cn

H. Yang
e-mail: hxyang@whu.edu.cn

ic details and electrochemical performance of the Pb-sandwiched composite nanoparticles used as the anode material for Li-ion batteries.

Experimental

Pb (99.0% purity, 200 mesh, National Medicine Co., Ltd., Shanghai, China), SiC (99.5% purity, 40–60 nm), and graphite (99% purity) were used as received. The SiC@Pb samples were prepared by high-energy ball milling (8000M Mixer/Mill, SPEX, USA) for 20 h, and then these samples were milled with graphite by a planetary mill (QM-1SP04, Nanjing, China) with a rotation speed of 240 rpm for 6 h to produce the SiC@Pb@C composite nanoparticles. The weight ratio of milling balls to the powder materials was maintained as 20:1. To prevent metal oxidation during milling, material handling was performed in a dry glove box with purified Ar atmosphere.

The crystalline structure of the as-prepared composites was characterized by X-ray diffraction on a Shimadzu X-ray diffractometer using Cu Kα radiation. X-ray photoelectron spectroscopy (XPS) measurements were carried out with a Kratos XSAM800 Ultra Spectrometer. The surface morphologies of the composite particles were characterized by scanning electron microscopy (Quanta 200, FEI, the Netherlands) and transmission electron microscopy (TEM, JEOL, JEM-2010-FEF).

Electrochemical testing of electrode materials was performed using coin cells with the SiC@Pb@C composite anode placed on a stainless steel current collector with lithium metal as the counter electrode. The electrolyte was 1 mol L^{-1} $LiPF_6$ dissolved in a mixture of ethylene carbonate, dimethyl carbonate, and diethyl carbonate (1:1:1 by weight, Zhangjiagang Guotai-Huarong New Chemical Materials Co., Ltd., China), and the separator was a microporous membrane (Celgard 2400). The composite anode was prepared by mixing 80 wt.% composite powder, 12 wt.% acetylene black, 4 wt.% carboxymethyl cellulose, and 4 wt.% styrene butadiene rubber together and dissolving the electrode mixture into distilled water to form a slurry, then coating the electrode slurry on nickel foam, pressing, and drying at 80 °C for 10 h under vacuum. SLK-2016 coin cells were then assembled in an argon-filled glove box and galvanostatically charged and discharged at a constant current density of 100 mA g^{-1} using a battery tester (Land CT2001A, Wuhan, China). Three different charge cutoff voltages of 2.0, 1.5, and 1.0 V were used, and the corresponding electrodes were denoted as SPC-1, SPC-2 and SPC-3, respectively. Cyclic voltammetric measurements were also carried out with the three-electrode cell at a scan rate of 0.1 mV s^{-1}.

Results and discussion

The X-ray diffraction (XRD) pattern of the as-prepared SiC@Pb@C particles with a mass ratio of SiC/Pb/C= 10:80:10 is shown in Fig. 1. Except for few weak XRD signals of PbO that may arise from a slight oxidation of the highly active Pb surface during ball milling, all the identified XRD peaks of the SiC@Pb@C nanocomposite can be indexed by tetragonal Pb (JCPDS no. 04-0686), cubic SiC (JCPDS no. 75-0254), and hexagonal graphite (JCPDS no. 75-2078). Compared with metallic Pb in Fig. 1, the XRD signals of the Pb in the SiC@Pb@C composite appeared evidently weaker and broader, implying a decrease in the crystallinity and size of the composite particles. When calculated based on the Scherer equation, the particle size of Pb decreased from micrometer to ~20 nm after ball milling. By dissolving the composite in acetic acid, the weight content of PbO in the composite was calculated to be 13%.

The surface morphology of the SiC@Pb@C nanocomposite was investigated by transmission electron microscopy. As is shown in Fig. 2a, it can be observed that the nanocomposite mainly comprises particles of ~100 nm in size (Fig. 2a). The TEM images of the particles in Fig. 2b, c further confirmed the formation of a sandwiched structure of the SiC@Pb@C and showed the clearly divided nanodomains: an outer carbon layer of ~10-nm thickness, a 10- to 20-nm-thick interlayer of Pb, and a SiC nanocore. The local magnified images in Fig. 2c (insets) show two lattice fringes corresponding to 2.87 Å of tetragonal Pb(111) plane in the middle layer and 3.25 Å of hexagonal graphite(111) plane in the outer layer, respectively. XPS analysis (Fig. 2d)

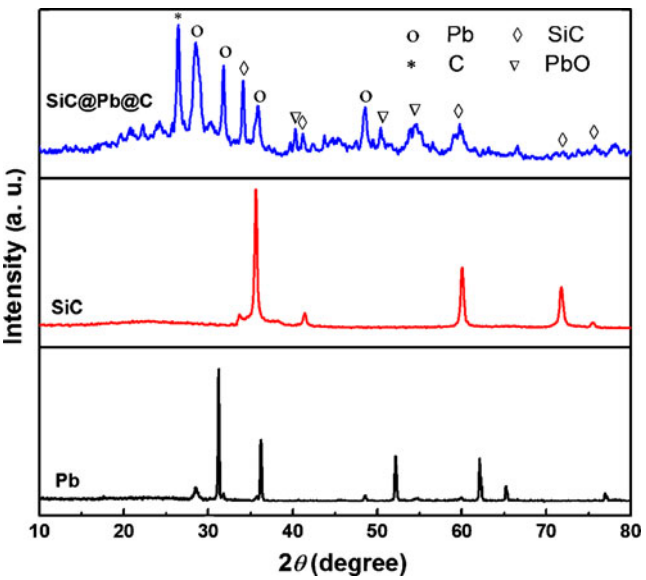

Fig. 1 XRD patterns of the SiC@Pb@C nanocomposite compared with pure SiC and metallic Pb

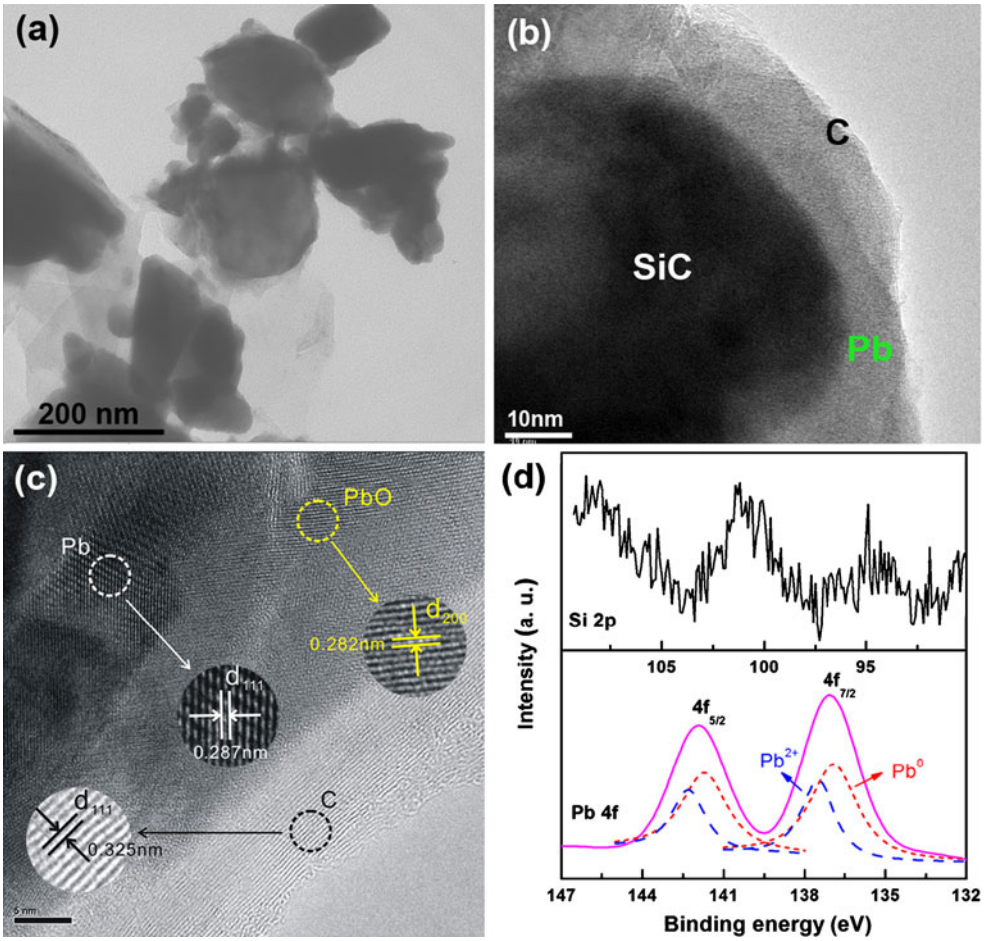

Fig. 2 **a**–**c** TEM images. **d** Binding energies of Pb 4*f* and Si 2*p* in the as-prepared SiC@Pb@C composite

revealed that the Pb $4f_{7/2}$ and $4f_{5/2}$ core peaks consist of two components. The first one at 136.9 and 141.7 eV is assigned to metallic Pb and the other one at 137.5 and 142.3 eV shows the presence of lead oxide (PbO) at the surface of the sample, in good agreement with the XRD (Fig. 1) and TEM (Fig. 2c) observations. However, the XPS signal of the Si 2*p* electrons (101.8 eV) shown in Fig. 2d was hardly detected, indicating that the SiC core was embedded in the composite so deeply that X-ray light cannot penetrate through the Pb layer. This sandwiched nanostructure was formed mainly because a cold welding process took place between Pb and SiC particles during the mechanical ball milling where ductile Pb was welded and pinned on the surface of rigid SiC particles by mechanical force; afterward, the SiC@Pb nanoparticles were coated by carbon. In this way, the inner core, SiC, can alleviate the huge volumetric change of the Pb anode, and the outer shell, graphite, cannot only enhance the lithium intercalation kinetics but also prevent the aggregation of the Pb nanoparticles.

The electrochemical performances of the SiC@Pb@C nanocomposite anode are shown in Figs. 3 and 4. Both the composite anode and the pure Pb anode were tested at a constant current density of 100 mA g^{-1}. Figure 3 shows the galvanostatic charge–discharge voltage profiles of the SPC-1 electrode. As can be seen, the composite anode delivered an initial reversible discharge capacity of 401 mAh g^{-1}, corresponding to 88% of its theoretical capacity. The initial Coulombic efficiency of the SiC@Pb@C electrode was 45.1%. This irreversible capacity loss most likely arose

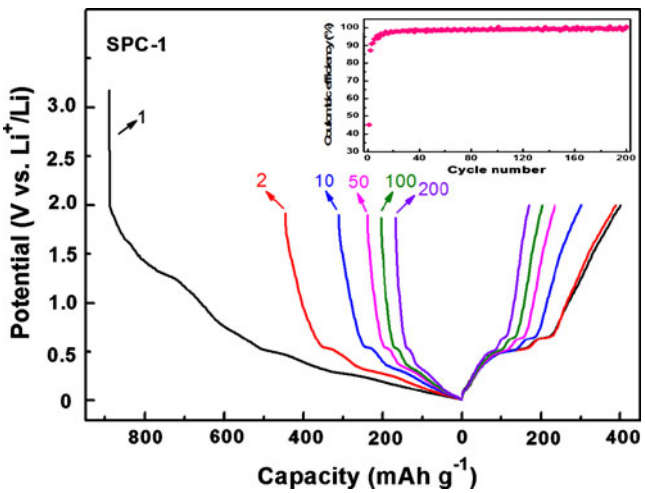

Fig. 3 Voltage profiles (Coulombic efficiency given as the *inset*) of the SPC-1 electrode

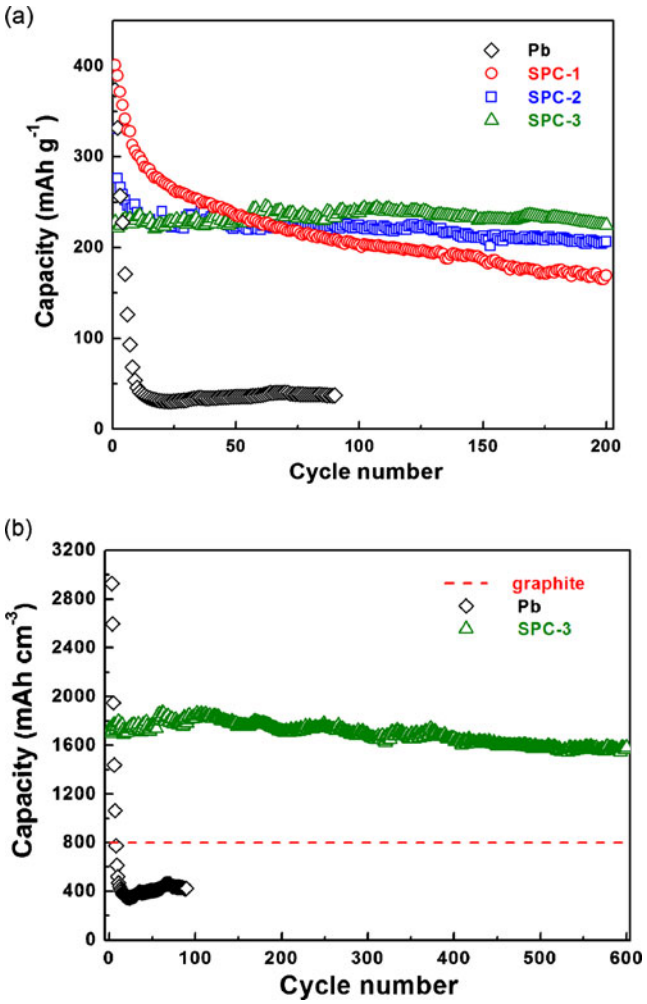

Fig. 4 **a** Gravimetric capacities of the SPC-1, SPC-2, SPC-3, and Pb electrodes. **b** Volumetric capacities of the SPC-3 and Pb electrodes

through two primary mechanisms: (1) decomposition of the electrolyte for the formation of SEI film on the active surface of the material and (2) reduction of the surface PbO. Nevertheless, the Coulombic efficiency of the electrode kept steadily above 95% after the fifth cycle, suggesting that this material is very electrochemically reversible. Particularly, the SPC-1 electrode in our work still delivers a capacity of 170 mAh g^{-1} up to 200 cycles, which is far superior to the cycling performance of the pure Pb electrode in Fig. 3.

It is commonly known that the voltage window selected in a charge–discharge experiment can greatly affect the cycling performance for an anode material. This was also demonstrated for the SiC@Pb@C material shown in Fig. 4a. When the cycling voltage interval was set at 0.005–1.5 V, the capacity retention for the SPC-2 electrode was significantly improved as compared with that cycled in the potential range between 0.005 and 2.0 V. Especially, when cycled in the potential range between 0.005 and 1.0 V, the SPC-3 electrode displayed an initial reversible capacity of 228 mAh g^{-1} with almost no capacity fade up to 200 cycles, exhibiting a significantly enhanced cycling performance in comparison with the previously reported Pb anode [19, 20]. Although its gravimetric capacity is slightly lower than that of commercial graphite, it has an extremely high volumetric capacity of over twice that of graphite (800 mAh g^{-1}). A reversible volumetric capacity of >1586 mAh cm^{-3} (the density of the composite is about 7.65 gcm^{-3}) can be maintained even after 600 cycles (Fig. 4b), which is comparable to that of the reported Sn-based and Si-based anodes [21, 22]. The improved cycling stability at narrower potential intervals is likely due to the existence of a residual Li_xPb film at a lowered charging potential limit [14], which was produced by an incomplete dealloying reaction of the lithiated phase. The Li_xPb film may act as a binder between the active Pb phase and the SiC core, thus preventing the pulverization and exfoliation of the Pb interlayer. Furthermore, this excellent electrochemical performance demonstrates that the SiC substrate is effective for buffering the volumetric changes during cycling, and the presence of the carbon shell not only supports the faster reaction of the electrode but also prevents the agglomeration of the Pb nanoparticles.

The improved cycling performance by cycling at narrower voltage windows was also validated by the cyclic voltammogram data of the SiC@Pb@C sample in different potential ranges. As is shown in Fig. 5, two reduction current peaks appeared around 1.5 and 1.1 V in the first cathodic scan for the composite electrode, featuring the irreversible reduction of PbO [14, 16]. In subsequent scans, two pairs of the redox peaks appeared at the potential of 0.2–0.60 V, corresponding to the formation of $Li_{2.6}Pb$ and

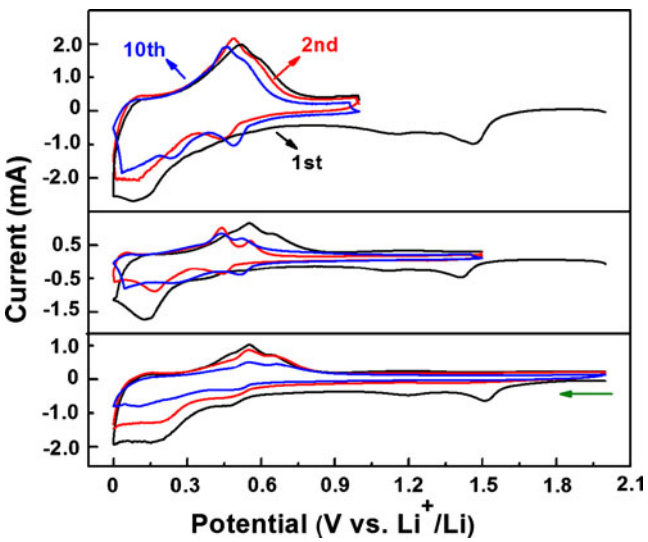

Fig. 5 Cyclic voltammograms of the SiC@Pb@C composite in different potential ranges

LiPb alloy [14], respectively. It is noteworthy that after ten cycles, the peak currents distinctly decreased when cycling the composite anode at wider potential range, while almost no noticeable change of the peak areas was observed in the potential range between 0.005 and 1.0 V, which is in good agreement with the charge–discharge voltage profiles of the composites.

Conclusions

A novel and exciting Pb-sandwiched nanocomposite anode material (SiC@Pb@C) was prepared through a simple ball milling route. The nanocomposite anode shows reversible volumetric capacity of >1586 mAh cm^{-3} (207 mAh g^{-1}) up to 600 cycles in the potential range between 0.005 and 1.0 V. This sandwiched structure helps buffer the volumetric changes during cycling. Based on this anode's high volumetric energy density, such a Pb-based composite may be one of the best anode candidates for lithium-ion batteries.

Acknowledgments We acknowledge financial support by the National Basic Research Program of China (2009CB220100) and the National Science Foundation of China (no. 20873095).

References

1. Huggins RA (1999) J Power Sources 82:13–19
2. Larcher D, Beattie S, Morcrette M, Edstroem K, Jumas JC, Tarascon JM (2007) J Mater Chem 17:3759–3772
3. Gao X-P, Yang H-X (2010) Energ Environ Sci 3:174
4. Magasinski A, Dixon P, Hertzberg B, Kvit A, Ayala J, Yushin G (2010) Nat Mater 9:353–358
5. Cho J (2010) J Mater Chem 20:4009–4014
6. Dong H, Ai XP, Yang HX (2003) Electrochem Commun 5:952–957
7. Yu Y, Gu L, Zhu CB, van Aken PA, Maier J (2009) J Am Chem Soc 131:15984–15985
8. Chen ZX, Qian JF, Ai XP, Cao YH, Yang HX (2009) J Power Sources 189:730–732
9. Huang L, Cai JS, He Y, Ke FS, Sun SG (2009) Electrochem Commun 11:950–953
10. Besenhard JO, Hess M, Komenda P (1990) Solid State Ionics 40–41:525–529
11. Benedek R, Thackeray MM (2002) J Power Sources 110:406–411
12. Needham SA, Wang GX, Konstantinov K, Tournayre Y, Lao Z, Liu HK (2006) Electrochem Solid-State Lett 9:A315–A319
13. Guo B, Liu N, Liu J, Shi H, Wang Z, Chen L (2007) Electrochem Solid-State Lett 10:A118–A121
14. Martos M, Morales J, Sanchez L (2003) Electrochim Acta 48:615–621
15. Liu ZL, Lee JY (2001) J Power Sources 97–98:247–250
16. Pan QM, Wang ZJ, Liu J, Yin GP, Gu M (2009) Electrochem Commun 11:917–920
17. Chen Z, Cao Y, Qian J, Ai X, Yang H (2010) J Phys Chem C 114:15196–15201
18. Chen Z, Cao Y, Qian J, Ai X, Yang H (2010) J Mater Chem 20:7266–7271
19. Ng SH, Wang J, Konstantinov K, Wexler D, Chen J, Liu HK (2006) J Electrochem Soc 153:A787–A793
20. Martos M, Morales J, Sanchez L, Ayouchi R, Leinen D, Martin F, Barrado JRR (2001) Electrochim Acta 46:2939–2948
21. Beattie SD, Larcher D, Morcrette M, Simon B, Tarascon JM (2008) J Electrochem Soc 155:A158–A163
22. Wang Y, Wu M, Jiao Z, Lee JY (2009) Chem Mater 21:3210–3215